GaTe-Sb2Te3 thin-films phase change characteristics

M. Bouska, Virginie Nazabal, J. Gutwirth, T. Halenkovic, J. Prikryl, S. Normani, P. Nemec

GaTe-Sb$_2$Te$_3$ thin films phase change characteristics

Marek Bouška,[1] **Virginie Nazabal,**[2,1] **Jan Gutwirth**[1], **Tomáš Halenkovič**[1], **Jan Přikryl**[3], **Simone Normani**[1], **Petr Němec**[1,*]

[1]*Department of Graphic Arts and Photophysics, Faculty of Chemical Technology, University of Pardubice, Studentská 573, 532 10 Pardubice, Czech Republic*
[2]*Institut des Sciences Chimiques de Rennes, UMR-CNRS 6226, Université de Rennes 1, Campus de Beaulieu, 35 042 Rennes Cedex, France*
[3]*Center of Materials and Nanotechnologies, Faculty of Chemical Technology, University of Pardubice, nám. Čs. legií 565, 530 02 Pardubice, Czech Republic*
*Corresponding author: petr.nemec@upce.cz

Radio-frequency magnetron co-sputtering technique exploiting GaTe and Sb$_2$Te$_3$ targets was used for the fabrication Ga-Sb-Te thin films. Prepared layers cover broad region of chemical composition (~10.0-26.3 at. % of Ga, ~19.9-34.4 at. % of Sb) while keeping Te content fairly constant (53.8-55.6 at. % of Te). Upon crystallization induced by annealing, large variations in electrical contrast was found, reaching sheet resistance ratio of R$_{annealed}$/R$_{as-deposited}$ ~2.2×10^{-8} for Ga$_{26.3}$Sb$_{19.9}$Te$_{53.8}$ layer. Phase transition from amorphous to crystalline state further leads to huge changes of optical functions demonstrated by optical contrast values up to $|\Delta n|+|\Delta k| =$ 4.20 for Ga$_{26.3}$Sb$_{19.9}$Te$_{53.8}$ composition.
© 2019 Optical Society of America

During the last decades, the thin films from Ge-Sb-Te and/or Ag- and In-doped Sb$_2$Te systems have been thoroughly investigated as depicted in Refs [1-6] and papers cited therein. The main scientific as well as technological interest of this group of inorganic materials is their ability to transform quickly and reversibly between amorphous and crystalline phases (disorder-order transition); this phenomenon was reported 50 years ago by Ovshinsky [7]. Phase transition can be reversibly induced through varying the electric field or temperature by heating *via* a laser pulse in optical recording applications [3, 8]. The remarkable properties of phase change materials based on Ge-Sb-Te are connected with changes of optical reflectivity (up to 30%) and/or electrical resistivity (several orders of magnitude) taking place upon phase transition [9].

Described phase change materials are exploited in commercial optical data storage media [1, 10] (digital versatile disks (DVD) or Blu-ray disks (BD) technologies) and considered in non-volatile memories and more recently in other photonic applications such as integrated all-photonic non-volatile memories, optical color rendering, nanopixel displays, and reconfigurable nanoplasmonic devices or active terahertz photonics [6, 11].

There were many attempts to improve the properties of phase change materials that have led to the modifications of chemical composition of Ge-Sb-Te materials in two ways. First, the changes in stoichiometry of basic materials were explored, i.e. apart from prototypical Ge$_2$Sb$_2$Te$_5$ composition, other Ge-Sb-Te compounds along the pseudobinary GeTe-Sb$_2$Te$_3$ tie line, such as Ge$_1$Sb$_2$Te$_4$, Ge$_8$Sb$_2$Te$_{11}$ etc. were investigated [10, 12]. The other way typically led through doping or alloying with another elements, for example with Sn or Se [13, 14]. It is worthy to mention a predictive approach for phase change materials suggested e.g. in Refs [4, 15].

Another approach is to deal with germanium-free phase change materials. Here, important examples, which need to be mentioned, are Sb-Te based materials and GaSb [1, 5, 16]. Among them, the binary family Sb-Te, centred around the eutectic Sb$_{70}$Te$_{30}$ is doped mainly with silver and indium forming the well-known AIST phase change material. Moreover, some materials compositions from ternary Ga-Sb-Te system and their phase transitions were studied in Refs [17-21]. Kao [19] used single cathode radio frequency (RF) magnetron sputtering with Ga$_2$Sb$_5$Te$_3$ target concluding that prepared thin films demonstrate a capability of three-level resistance changes in a single memory unit. The other authors exploited magnetron co-sputtering with GaSb and Sb$_2$Te$_3$ [17, 21] or Sb$_7$Te$_3$ [17], Sb$_8$Te$_2$ [18], Sb/Te [20] targets for the deposition of thin films (usually with high content of Sb) resulting in high crystallization speed, good electrical contrast between amorphous and crystalline phase (up to approximately five orders of magnitude) and generally promising characteristics for phase change memories. Particularly, Cheng pointed out remarkable properties for stoichiometric Ga$_4$Sb$_6$Te$_3$ layers [20]. Later on, alloy of this composition was studied via first-principles molecular dynamics simulations to address the structural features of the amorphous phase [22].

Based on above-mentioned facts, the aim of this work is to combine RF magnetron co-sputtering as an advanced technique for thin films growth with the fabrication of phase change memory materials represented by Ga-Sb-Te thin films, as an alternative to Ge-Sb-Te system. Co-sputtering deposition method was employed for its cost-efficiency to fabricate thin films of wide range of chemical compositions. Moreover, co-sputtering is an efficient

deposition technique to fabricate amorphous thin films whose composition is out of the glass-forming region of the system under study. However, contrary to previously published reports with Sb-rich compositions, we used different strategy that is to sputter GaTe and Sb_2Te_3 targets leading to films fabrication with higher Ga and Te content. Furthermore, in addition to studying the electrical contrast, we focused on the characterization of optical properties in order to describe and compare optical contrast (in terms of $\Delta n+i\Delta k$, where n and k stand for refractive index and extinction coefficient, respectively) of fabricated Ga-Sb-Te thin films.

The RF magnetron co-sputtering of Ga-Sb-Te thin films was performed at a room temperature using MPE600 multi-chamber deposition system (Plassys-Bestek) which is equipped with symmetrically arranged confocal deposition cluster consisting of three cathodes [23, 24]. Two polycrystalline 2" 99.999 % targets with the composition of GaTe and Sb_2Te_3 (ALB Materials, Inc., USA) were used. Thin films were deposited on borosilicate glass and single crystalline silicon wafers <100> substrates. The experimental conditions were kept constant throughout all the depositions, *i.e.* background pressure of $\leq 5\times10^{-7}$ mbar, argon working pressure of 5×10^{-3} mbar maintained by 75 sscm flow rate and substrate-target distance of about 8 cm with substrate holder rotation. To study the effect of crystallization, as-deposited films were annealed in inert atmosphere (pure argon) at the temperature of 300 °C (to assure that the crystallization proceeded) for 120 min and slowly cooled down to room temperature.

The morphology and the chemical composition of films was checked by scanning electron microscopy (SEM, JEOL JSM 6400) linked with an energy-dispersive X-ray spectroscopy (EDS) analyzer. Atomic force microscopy (AFM, Solver NEXT, NT-MDT) was used to study topography of Ga-Sb-Te layers within scanned area of 2 μm x 2 μm in a semi-contact mode. X-ray diffraction (XRD) technique (D8-Advance diffractometer, Bruker AXS) was exploited to determine the structure of Ga-Sb-Te samples using Bragg–Brentano θ–θ geometry with CuKα radiation and secondary graphite monochromator. The diffraction angles were measured at room temperature from 5 to 65° (2θ) within 0.02° steps. Sheet resistance temperature dependences measurements were carried out using a four-point probe based on van der Pauw method [25].

Optical properties were investigated using spectroscopic ellipsometry (VASE, J. A. Woollam Co.) within the spectral range of 300-2500 nm, measuring 100 revolutions with wavelengths steps of 20 nm at selected angles of incidence (50°, 60°, and 70°).

For the analysis of ellipsometry data of as-deposited layers, we used Cody-Lorentz (CL) model which includes the correct band edge function, weak Urbach absorption tail description as well as Lorentz oscillator function [26]; this model is suitable for the description of amorphous chalcogenides optical functions [27, 28]. In case of as-deposited GaTe thin film, CL model did not give reasonable results, so that model exploiting Kramers-Kronig consistent parametric semiconductor oscillator (developed initially for the analysis of compound semiconductor films [29]) was preferably employed. In case of annealed layers, a model describing chalcogenide thin films' dielectric functions consisted of parametric semiconductor oscillator and Lorentz oscillator.

The chemical composition of fabricated Ga-Sb-Te films estimated by EDS is visualized in the ternary diagram in Fig. 1 as well as in Table 1. In comparison with the nominal composition, the as-

deposited films sputtered from single targets at RF power of 20 W are only slightly overstoichiometric in Ga or Sb content (+2.9 at. % for Ga, +2.4 at. % for Sb). For co-sputtered layers (sum of RF power applied to both targets was fixed at 30 W), broad range of composition was successfully covered (~10.0-26.3 at. % of Ga, ~19.9-34.4 at. % of Sb) with only slight variation in Te content (53.8-55.6 at. % of Te) by varying RF power on the two cathodes in the range of 11-19 W.
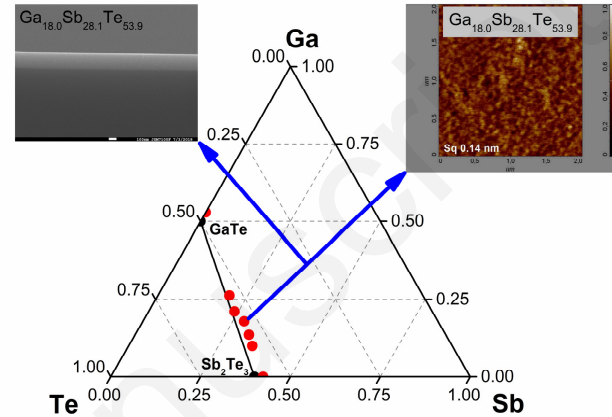

Fig. 1. Ternary Ga-Sb-Te diagram with indicated positions of (co-)sputtered thin films' composition (red symbols) and targets' composition (black symbols). Right inset illustrates AFM scan (2 μm × 2 μm) with indicated RMS roughness value Sq of $Ga_{18.0}Sb_{28.1}Te_{53.9}$ thin film. Left inset shows SEM micrograph of cross-section of the same film.

Table 1 Summary of co-sputtered Ga-Sb-Te thin films: chemical composition (± 1 at. %) evaluated by EDS, band gap values in as-deposited state (E_g, ±0.02 eV), electrical contrast values (in terms of sheet resistance ratio $R_{annealed}/R_{as-deposited}$), thickness ratio ($d_{annealed}/d_{as-deposited}$) between annealed and as-deposited state, optical contrast $\Delta n+i\Delta k$ ($n,k(annealed)-n,k(as-deposited)$) values at wavelength of 400 nm, and its absolute values. Note that the error in determination of films' thickness is ±2 nm.

Composition (at. %)	E_g (eV)	$R_{ann.}/R_{as-dep.}$	$d_{ann.}/d_{as-dep.}$	$\Delta n+i\Delta k$ @400 nm	$\|\Delta n\|+\|\Delta k\|$ @400 nm
$Ga_{53}Te_{47}$	-	3.5×10^{-5}	0.902	-0.27-i0.75	1.02
$Ga_{26}Sb_{20}Te_{54}$	0.90	2.2×10^{-8}	0.776	-2.80-i1.40	4.20
$Ga_{21}Sb_{24}Te_{55}$	0.81	2.5×10^{-7}	0.811	-2.61-i0.36	2.97
$Ga_{18}Sb_{28}Te_{54}$	0.76	5.4×10^{-7}	0.823	-2.05-i0.18	2.23
$Ga_{14}Sb_{32}Te_{56}$	0.71	1.5×10^{-6}	0.889	-1.84+i0.40	2.24
$Ga_{10}Sb_{34}Te_{56}$	0.66	3.0×10^{-6}	0.839	-2.02+i0.38	2.40
$Sb_{42}Te_{58}$	0.46	9.9×10^{-3}	0.966	-0.79-i0.57	1.36

Thin films fabricated by (co-)sputtering technique were homogeneous and amorphous as confirmed by optical/electron microscopy, except of sputtered GaTe and Sb_2Te_3 films which were partially crystalline (traces of hexagonal Te in case of GaTe film, rhombohedral Sb_2Te_3 in Sb_2Te_3 films) as determined from XRD

patterns. On annealing of GaTe films, hexagonal Te and/or Ga_2Te_5 crystalline phases are formed. The annealing of Sb_2Te_3 layers leads to the formation of rhombohedral Sb_2Te_3. With increasing concentration of Sb_2Te_3 in annealed Ga-Sb-Te thin films, the content of rhombohedral Sb_2Te_3 crystallites, their size, and preferential orientation in the layers grow. Co-sputtered Ga-Sb-Te films after annealing may also contain hexagonal Te and/or Ga_2Te_5 phases but they are not clearly distinguished.

The films' morphology studied *via* SEM, depicted as inset of Fig. 1, showed smooth surface of deposited films without any significant defects. For all as-deposited thin films, root mean squared roughness values (Sq) determined by AFM (exemplified as inset in Fig. 1) were found to be ≤0.4 nm confirming smooth surface of the layers. Contrary, films' roughness determined by AFM for annealed layers increased (up to ~10.8 nm for Sb_2Te_3 films) which is consistent with the crystallization of the films upon annealing.

In order to reveal electrical contrast between annealed and as-deposited thin films (in terms of sheet resistance data), temperature dependences of sheet resistance were measured (Fig. 2). Resulting electrical contrast values are given in Table 1 showing broad range over several orders of magnitude. Lowest electrical contrast values are observed for sputtered binary GaTe and Sb_2Te_3 layers. With growing content of Ga in co-sputtered Ga-Sb-Te thin films, the electrical contrast is increasing up to $R_{annealed}/R_{as-deposited}$ ~2.2×10^{-8} for $Ga_{26.3}Sb_{19.9}Te_{53.8}$ layers.
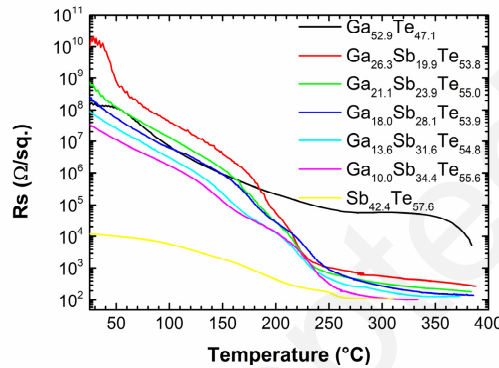

Fig. 2. Sheet resistance of as-deposited Ga-Sb-Te layers temperature dependence (heating rate of 2 °C.min^{-1}).

The thickness of the as-deposited samples under study, determined by ellipsometry data analysis, was in the range of ~170-240 nm (which enables easy implementation of spectroscopic ellipsometry data analysis). On the other hand, the thickness of annealed layers was ~3-22% lower in comparison with the thicknesses of as-deposited ones (Table 1); such thickness changes are substantially larger when compared to Ge-Sb-Te thin films (~3-13% for pulsed lased deposited layers [12, 30]). The largest thickness decrease upon annealing of as-deposited Ga-Sb-Te thin films has been revealed for $Ga_{26.3}Sb_{19.9}Te_{53.8}$ composition.

Application of CL model for ellipsometry data analysis allowed the determination of band gap (E_g) values of as-deposited films (Table 1). Layered GaTe with a monoclinic structure and a direct bandgap of about 1.7 eV at the Z point of the Brillouin zone border was reported earlier [31, 32]. Sb_2Te_3 is a semiconductor with

optical bandgap of ~0.52-0.80 eV in amorphous state and bandgap energies of ~0.15-0.32 eV in crystalline state [30]. We note that E_g calculated in this work for sputtered as-deposited Sb_2Te_3 layer (~0.46 eV) is consistent with data found in the literature and with the fact that the layer is partially crystalline. The E_g values of co-sputtered Ga-Sb-Te thin films lie between those of GaTe and Sb_2Te_3 thin films, logically tending to decrease with a growing content of Sb_2Te_3 in the films (Table 1).

Best fit optical functions, i.e. refractive index and extinction coefficient spectral dependences, deducted from spectroscopic ellipsometry data analysis for both, the as-deposited and annealed Ga-Sb-Te thin films are shown in Figs 3 and 4, respectively. As it follows from Figs 3 and 4, in studied spectral and compositional region, the refractive index and extinction coefficient vary drastically. To assess the refractive index and extinction coefficient changes, optical contrast $\Delta n+i\Delta k$ ($n,k(annealed)-n,k(as-deposited)$) values at wavelength of 400 nm (at working wavelength of BD which is 405 nm) and absolute values of optical contrast at 400 nm in terms of $|\Delta n|+|\Delta k|$ were extracted (Table 1). Lowest values of optical contrast as well as its absolute value were found for binary GaTe ($\Delta n+i\Delta k$ = -0.27-i0.75, $|\Delta n|+|\Delta k|$ = 1.02) and Sb_2Te_3 ($\Delta n+i\Delta k$ = -0.79-i0.57, $|\Delta n|+|\Delta k|$ = 1.36) sputtered telluride layers. Contrary, co-sputtered Ga-Sb-Te films show much larger optical contrast reaching values of $\Delta n+i\Delta k$ = -2.80-i1.40 and $|\Delta n|+|\Delta k|$ = 4.20 for $Ga_{26.3}Sb_{19.9}Te_{53.8}$ composition. When compared with data determined for $Ge_2Sb_2Te_5$ ($\Delta n+i\Delta k$ = -1.20+i1.05, giving $|\Delta n|+|\Delta k|$ = 2.25) and $Ge_8Sb_2Te_{11}$ ($\Delta n+i\Delta k$ = -1.48+i1.35, resulting in $|\Delta n|+|\Delta k|$ = 2.83) by Yamada [10], Ga-Sb-Te layers present comparable and even larger values, especially for films richer in gallium.
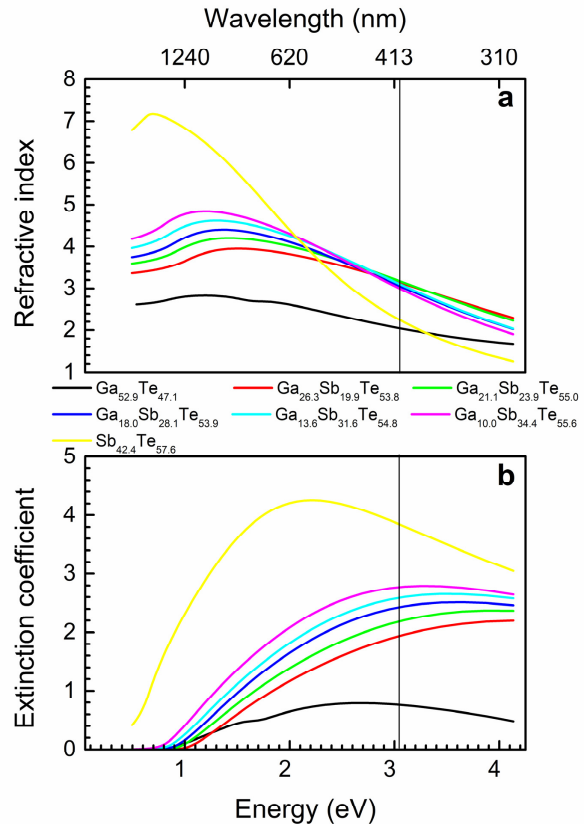
Fig. 3. Optical functions of as-deposited (co-)sputtered Ga-Sb-Te thin films: (a) spectral dependences of refractive indices, (b) spectral dependences of extinction coefficients. Vertical lines represent wavelength of 405 nm used in BD technology.
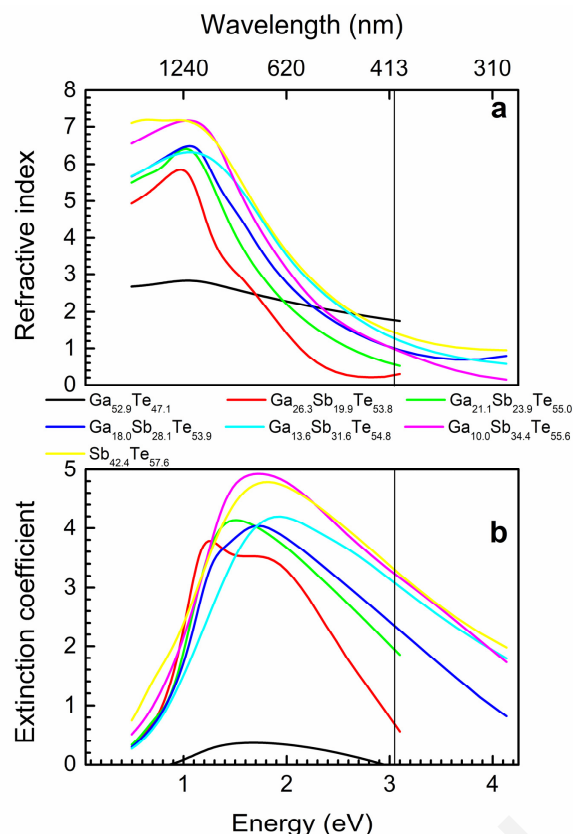

Fig. 4. Optical functions of annealed (co-)sputtered Ga-Sb-Te thin films: (a) spectral dependences of refractive indices, (b) spectral dependences of extinction coefficients. Vertical lines represent wavelength of 405 nm used in BD technology.

To conclude, the study of fabrication and characterization of various properties of co-sputtered Ga-Sb-Te thin films was presented. The used deposition technique allowed to prepared thin films with compositions in a wide range. Spectroscopic ellipsometry data analysis showed large values of optical contrast, which are comparable or higher than that ones reported for Ge-Sb-Te system. Based on achieved results, co-sputtered thin films from Ga-Sb-Te system seem to be prospective for the potential applications in the field of phase change memory materials. This is why we plan to expand this Letter in two directions: new compositions as well as other important characterization techniques which will help to understand the structure of the layers as well as structure-properties relation.

Disclosures. The authors declare no conflicts of interest.

References

1. M. Wuttig and N. Yamada, Nat. Mater. **6**, 824-832 (2007).
2. G. W. Burr, M. J. Breitwisch, M. Franceschini, D. Garetto, K. Gopalakrishnan, B. Jackson, B. Kurdi, C. Lam, L. A. Lastras, A. Padilla, B. Rajendran, S. Raoux, and R. S. Shenoy, Journal of Vacuum Science & Technology B **28**, 223-262 (2010).
3. S. Raoux, W. Welnic, and D. Ielmini, Chemical Reviews **110**, 240-267 (2010).
4. D. Lencer, M. Salinga, and M. Wuttig, Adv. Mater. **23**, 2030-2058 (2011).
5. V. L. Deringer, R. Dronskowski, and M. Wuttig, Adv. Funct. Mater. **25**, 6343-6359 (2015).
6. W. Zhang, R. Mazzarello, M. Wuttig, and E. Ma, Nat. Rev. Mater. **4**, 150-168 (2019).
7. S. R. Ovshinsky, Phys. Rev. Lett. **21**, 1450-1453 (1968).
8. I. Friedrich, V. Weidenhof, W. Njoroge, P. Franz, and M. Wuttig, J. Appl. Phys. **87**, 4130-4134 (2000).
9. W. Welnic and M. Wuttig, Materials Today **11**, 20-27 (2008).
10. N. Yamada, Phys. Status Solidi B-Basic Solid State Phys. **249**, 1837-1842 (2012).
11. M. Wuttig, H. Bhaskaran, and T. Taubner, Nature Photonics **11**, 465-476 (2017).
12. M. Bouska, S. Pechev, Q. Simon, R. Boidin, V. Nazabal, J. Gutwirth, E. Baudet, and P. Nemec, Scientific Reports **6**, 26552 (2016).
13. S. Buller, C. Koch, W. Bensch, P. Zalden, R. Sittner, S. Kremers, M. Wuttig, U. Schuermann, L. Kienle, T. Leichtweiss, J. Janek, and B. Schoenborn, Chem. Mat. **24**, 3582-3590 (2012).
14. Y. F. Zhang, J. B. Chou, J. Y. Li, H. S. Li, Q. Y. Du, A. Yadav, S. Zhou, M. Y. Shalaginov, Z. R. Fang, H. K. Zhong, C. Roberts, P. Robinson, B. Bohlin, C. Rios, H. T. Lin, M. Kang, T. Gu, J. Warner, V. Liberman, K. Richardson, and J. J. Hu, Nature Communications **10**, 4279 (2019).
15. D. Lencer, M. Salinga, B. Grabowski, T. Hickel, J. Neugebauer, and M. Wuttig, Nat. Mater. **7**, 972-977 (2008).
16. L. van Pieterson, M. H. R. Lankhorst, M. van Schijndel, A. E. T. Kuiper, and J. H. J. Roosen, J. Appl. Phys. **97**, 083520 (2005).
17. C. M. Lee, W. S. Yen, J. P. Chen, and T. S. Chin, IEEE Trans. Magn. **41**, 1022-1024 (2005).
18. H. Y. Cheng, K. F. Kao, C. M. Lee, and T. S. Chin, IEEE Trans. Magn. **43**, 927-929 (2007).
19. K. F. Kao, C. M. Lee, M. J. Chen, M. J. Tsai, and T. S. Chin, Adv. Mater. **21**, 1695-1699 (2009).
20. H. Y. Cheng, S. Raoux, and J. L. Jordan-Sweet, Appl. Phys. Lett. **98**, 121911 (2011).
21. Y. G. Lu, S. N. Song, Z. T. Song, W. C. Ren, Y. Cheng, and B. Liu, Applied Physics Express **4**, 094102 (2011).
22. A. Bouzid, S. Gabardi, C. Massobrio, M. Boero, and M. Bernasconi, Phys. Rev. B **91**, 184201 (2015).
23. T. Halenkovic, J. Gutwirth, P. Nemec, E. Baudet, M. Specht, Y. Gueguen, J. C. Sangleboeuf, and V. Nazabal, J. Am. Ceram. Soc. **101**, 2877-2887 (2018).
24. R. Mawale, T. Halenkovic, M. Bouska, J. Gutwirth, V. Nazabal, P. L. Bora, L. Pecinka, L. Prokes, J. Havel, and P. Nemec, Scientific Reports **9**, 10213 (2019).
25. L. J. Van der Pauw, Philips Research Reports **13**, 1-9 (1958).
26. G. D. Cody, in *Semiconductors and semimetals*, J. I. Pankove, ed. (Academic, Orlando, FL, 1984), p. 11.
27. E. Baudet, A. Gutierrez-Arroyo, P. Nemec, L. Bodiou, J. Lemaitre, O. De Sagazan, H. Lhermitte, E. Rinnert, K. Michel, B. Bureau, J. Charrier, and V. Nazabal, Optical Materials Express **6**, 2616-2627 (2016).
28. E. Baudet, M. Sergent, P. Nemec, C. Cardinaud, E. Rinnert, K. Michel, L. Jouany, B. Bureau, and V. Nazabal, Scientific Reports **7**, 3500 (2017).
29. B. Johs, C. M. Herzinger, J. H. Dinan, A. Cornfeld, and J. D. Benson, Thin Solid Films **313**, 137-142 (1998).
30. P. Nemec, J. Prikryl, V. Nazabal, and M. Frumar, J. Appl. Phys. **109**, 073520 (2011).
31. S. X. Huang, S. Tatsumi, X. Ling, H. H. Guo, Z. Q. Wang, G. Watson, A. A. Puretzky, D. B. Geohegan, J. Kong, J. Li, T. Yang, R. Saito, and M. S. Dresselhaus, ACS Nano **10**, 8964-8972 (2016).
32. J. F. Sanchez-Royo, J. Pellicer-Porres, A. Segura, V. Munoz-Sanjose, G. Tobias, P. Ordejon, E. Canadell, and Y. Huttel, Phys. Rev. B **65**, 115201 (2002).